Observation of Deflection of a Beam of Multi-GeV Electrons by a Thin Crystal

U. Wienands,* T. W. Markiewicz, J. Nelson, R. J. Noble, and J. L. Turner
SLAC National Accelerator Laboratory, 2575 Sand Hill Road, Menlo Park, California 94025, USA

U. I. Uggerhøj and T. N. Wistisen
Department of Physics and Astronomy, University of Aarhus, Ny Munkegade 120, DK-8000 Aarhus, Denmark

E. Bagli, L. Bandiera, G. Germogli, V. Guidi, and A. Mazzolari
Department of Physics and Earth Sciences of the University of Ferrara, and INFN Section of Ferrara, Via Saragat 1/C, I-44122 Ferrara, Italy

R. Holtzapple and M. Miller
California Polytechnic State University, San Luis Obispo, California 93407, USA
(Received 6 May 2014; published 19 February 2015)

We report on an experiment performing channeling and volume reflection of a high-energy electron beam using a quasimosaic, bent silicon (111) crystal at the End Station A Test Beam at SLAC. The experiment uses beams of 3.35 and 6.3 GeV. In the channeling orientation, deflections of the beam of 400 μrad for both energies with about 22% efficiency are observed, while in the volume-reflection orientation, deflection of the beam by 120 μrad at 3.35 GeV and by 80 μrad at 6.3 GeV is observed with 86%–95% efficiency. Quantitative measurements of the channeling efficiency, surface transmission, and dechanneling length are taken. These are the first quantitative measurements of channeling and volume reflection using a primary beam of multi-GeV electrons.

DOI: 10.1103/PhysRevLett.114.074801 PACS numbers: 41.85.Ct, 61.85.+p

Channeling of protons in bent crystals has been investigated for many years and has led to experiments and applications in beam extraction and beam collimation [1–6]. A wealth of data exists for protons, spanning the energy range from MeV to almost a TeV. As a consequence, proton channeling and volume reflection (VR) are reasonably well understood. Comparatively few experiments studying channeling of electrons in bent crystals have been performed, mostly with beams of relatively low energy up to about 1 GeV [7,8] or in particle-counting experiments using secondary beams above 100 GeV [9–13] (some of which used negative pions).

However, there is interest in the possibility of applying crystals for beam collimation of high-energy electron (and positron) beams. In the International Linear Collider (ILC) [14,15], e.g., using a short silicon crystal instead of a longer amorphous spoiler would diminish wakefield effects and thus emittance dilution. Since bent crystals cause deflection of the scraped-off beam rather than random scattering, an increase in collimation efficiency at reduced overall length of the system can be expected. With a bunched beam with parameters comparable to those of a high-energy collider facility this experiment can be considered a milestone experiment in studying the manipulation of electron beams with bent crystals. Even though the energies used here are far below the ILC energy, our results provide important dependencies and scaling relations that narrow the range of parameters involved in a collimation system for high-energy electrons. New initiatives towards very high energy lepton colliders [16–18] would benefit from the application of this technology as well. A recent potential application has emerged for the LCLS-II project at SLAC. The challenge is to reduce dark-current beam loss by a factor of 10^7 to protect the undulator from radiation damage [19]. Adding bent crystals to the collimation system could reduce the radiation on the undulator by an additional factor of up to 10. This application involves beam energies up to a few GeV so the results presented here are directly applicable.

Application of crystals in the generation of x rays and γ rays using electrons is holding significant promise [20–22]. There are also a number of predictions from theory and simulations of the channeling efficiency, dechanneling length, and surface transmission of electrons [23] that at present can only be compared to data below 1 GeV as the high-energy experiments have not published quantitative results for these parameters. The measurements described in this Letter are a first step towards improving this situation.

The silicon (Si) crystal used in this experiment was fabricated at the Sensors and Semiconductor Laboratory at the University of Ferrara with the crystallographic orientation chosen to produce quasimosaic bending of the (111) plane [24]. Its thickness was measured interferometrically to be 60 ± 1 μm. The lateral size (about 22 mm wide) was optimized in order to reduce the anticlastic deformation

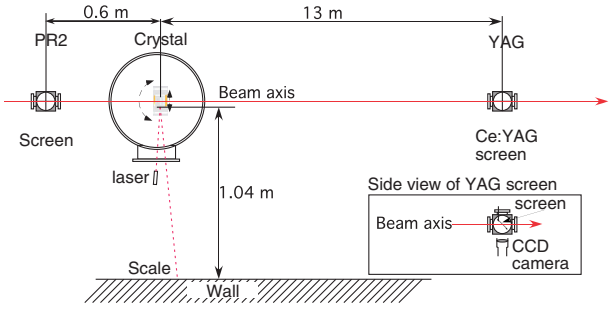

FIG. 1 (color online). Top view layout of the experiment.

caused by the bending. The (111) plane has a bending radius of 0.15 m for a bending angle (equals channeling angle) of $\theta_c = 402 \pm 9$ μrad in the horizontal direction. The critical angle, the maximum angle a particle can have against the atomic plane for channeling to still be possible, was calculated using the Doyle-Turner potential [25] to be $\theta_{\mathrm{crit}} = 115$ μrad at 3.35 GeV and $\theta_{\mathrm{crit}} = 80$ μrad at 6.3 GeV. The crystal was mounted in a scattering chamber in the End Station A Test Beam [26]. Figure 1 shows the experimental layout.

A rotational stage allows rotation of the crystal with step sizes nominally down to 5 μrad. A translational stage allows moving the crystal into the beam as well as selecting the position where the beam intercepts the crystal. A flat mirror mounted on the side of the crystal holder reflecting a laser beam to a screen at about 1 m distance provides a simple yet effective readout of the crystal angle with a resolution below 5 μrad. A cerium-doped yttrium aluminum garnet (YAG) screen of 500 μm thickness with a CCD camera 13 m downstream of the crystal provides the main diagnostics detecting the effect of the crystal on the beam. The YAG screen is pitched by 45° towards the camera, which is looking up from below the beam line. It was calibrated using the known diameter of the screen resulting in a resolution of about 28 pixels/mm in the horizontal direction, and 20 pixels/mm in the vertical direction. The thickness of the screen may lead to blurring corresponding to up to 25 μrad, which can affect the resolution in Fig. 7; the other figures all integrate over the vertical dimension and are not affected by this. The saturation behavior of YAG screens has been studied [27,28]; compared to their studies our charge density is down by a factor exceeding 100. Quantitative analysis using the formulas given in the references indicate a worst-case saturation of 5%. The camera is linear but saturates hard at 255 counts; we carefully adjusted the camera gain to avoid this.

End Station A receives the beam from the SLAC linac at up to 5 pulses/ sec. The optics was set to zero dispersion at the YAG screen and a beam width of < 150 μm (1σ) in the vertical and horizontal plane, after collimation. The beam divergence was inferred from wire scans to be less than 10 μrad. The intensity of the collimated beam was about

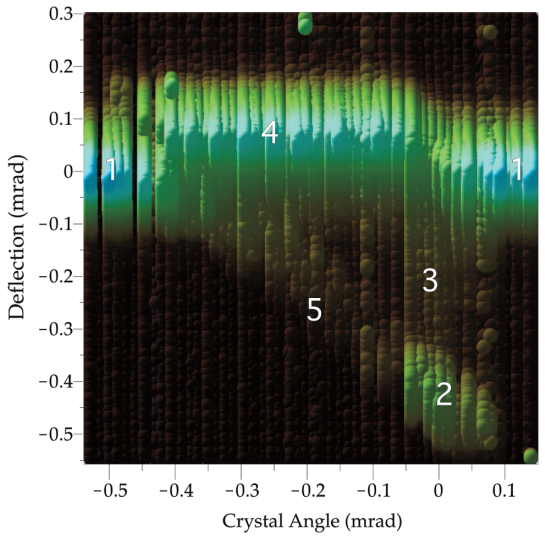

FIG. 2 (color online). Deflection plot at 6.3 GeV beam energy. Colors correspond to log(intensity). The numbers denote the orientation of the crystal. 1: amorphous. 2: channeling. 3: dechanneling. 4: volume reflection. 5: volume capture.

10^8 electrons per pulse. An insertable screen upstream of the crystal together with the YAG screen allowed us to maintain the beam position and angle on the crystal at all times.

The channeling condition of trapping particles between the crystalline planes, thus deflecting them with the crystal bending angle, is indicated by the appearance of a second beam spot on the YAG screen accounting for about 20% of the intensity. A dechanneling tail extends from the main peak towards the channeling peak. Volume reflection, particles bouncing off a crystalline plane in the opposite direction as the bending, shows itself as a lateral move of essentially the whole beam to the opposite side.

The deflection plot was obtained by rotating the crystal in small steps in the beam. It is shown in Fig. 2 for 6.3 GeV beam energy. From this plot, and a similar one for 3.35 GeV, the angle for maximum channeled intensity was determined to be 400 μrad at both energies, consistent with the crystal bending angle. The volume-reflection angle is 120 μrad for 3.35 GeV and 80 μrad for 6.3 GeV beam energy. A certain amount of volume capture—particles trapped in a channel rather than bouncing off a plane—is evident in Fig 2 as well, cautiously estimated at 5% to 10%.

After dark-frame subtraction a 5.5° rotation is removed and the horizontal intensity profile is extracted, averaging over a vertical height sufficient to cover the full extent of the beam spots. Only images with intensity above 1/3 of maximum intensity are used in the analysis. The intensity distributions obtained thus are fit with a function composed of three parts: a Gaussian each to describe the channeling peak as well as the nondeflected or volume-reflected peak,

and an exponential decay describing the dechanneling tail. The dechanneling rate is taken proportional to the population of particles in the channel that leads to the exponential decay in the intensity as the beam passes through the crystal with a characteristic decay length, i.e.,

$$\frac{dn(s)}{ds} = -\frac{n_0}{L_d}\exp\left(-\frac{s}{L_d}\right) = -\frac{n_0}{L_d}\exp\left(-\frac{\theta}{\theta_d}\right), \quad (1)$$

where $n(s)$ is the number of particles left in the channel, $n_0 = n(0)$, $L_d = \theta_d L_c/\theta_c$ is the dechanneling length, and s is the path length into the crystal; θ is the deflection angle. This simple model is underlying many dechanneling lengths quoted in the literature (e.g., Refs. [7,29]). In our analysis we convolve the dechanneling tail with the multiple scattering angle. The dechanneling tail function is then

$$F(\theta) = -A_t/4\left[\mathrm{erf}\left(\frac{({\sigma_1}^2 + \theta\theta_d - \theta_1\theta_d)}{\sqrt{2}\sigma_1\theta_d}\right) - 1\right]\sigma_1\sqrt{\pi}\mathrm{e}^{({\sigma_1}^2+2\theta\theta_d-2\theta_1\theta_d)/2{\theta_d}^2}\left[1 + \mathrm{erf}\left(\frac{({\sigma_2}^2 + \theta\theta_d - \theta_2\theta_d)}{\sqrt{2}\sigma_2\theta_d}\right)\right], \quad (2)$$

where A_t, θ_d are the intensity and the dechanneling length, θ_1 and θ_2 are the deflection angles of main and channeling peak, respectively, and σ_1 and σ_2 are the widths of the undeflected and the channeling peak. The channel is populated by the particles entering the crystal, reduced by the surface transmission (the fraction of particles initially captured in the channel). Figures 3 and 4 show examples of the fits obtained together with the individual contributions. Note that the fits do not constrain the area under the curves for the individual contributions with respect to each other. From the fit parameters we calculate the channeling efficiency, the surface transmission, and the dechanneling length.

An effort was made to understand parameter correlations and their effect on the extracted numbers. The strongest correlation was identified to exist between the dechanneling length and the width of the undeflected or volume-reflected peak. We studied the effect of saturation of the YAG screen on the results by folding the data with an experimental saturation function [27] and found the effect on the parameters to be below 1% when assuming 5% saturation. There is some evidence in the data suggesting that a tail (beyond Gaussian) may exist for the undeflected or volume-reflected peak. The effect of such a tail consistent with the measured profiles was assessed to be about a 10% increase in the value of the dechanneling length extracted, which we take as an additional systematic uncertainty. The data set described here is not exhaustive enough to clearly establish the presence and shape of such a tail.

The channeling efficiency is 22% at both energies with little indication of energy dependence. The VR angle is consistent with $1/\sqrt{\text{energy}}$ behavior. The experimental VR angle is essentially the same as the critical angle, somewhat in contrast to $\approx 0.8 \times \theta_{\text{crit}}$ seen in other experiments with negatively charged particles [10,30]. The surface transmission is measured to be 64% at 3.35 GeV, and 57% at 6.3 GeV, in very good agreement with our analytic estimates. The dechanneling length versus crystal angle at 6.3 GeV is shown in Fig. 5; it indicates that for the volume-captured particles the dechanneling length is shorter by roughly a factor of 2. We suggest this to be an indication of preferential population of higher-lying energy states by the volume-captured particles, with higher probability to dechannel than the lower-lying states.

The VR efficiency is the content of the main (reflected) peak as a fraction of the whole intensity. This definition gives somewhat lower numbers than one might expect,

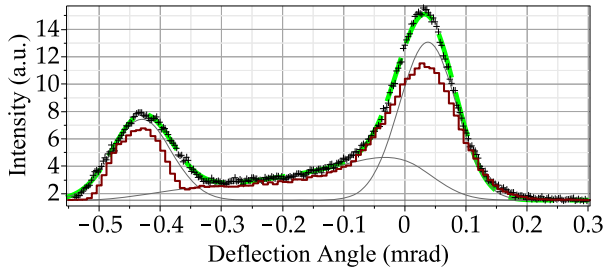

FIG. 3 (color online). Example of the fit to 6.3 GeV channeling data at 0 mrad crystal angle. The dashed line (green) is the fitted function; the crosses are the measured intensity. The solid dark-gray lines represent the individual contributions to the fit (Gaussian peaks, dechanneling tail, and constant background). For this example, the channeling efficiency is 23.8%, the surface transmission is 55%, and the dechanneling length is 33 μm. The maroon histogram is from DYNECHARM++ simulations, see text.

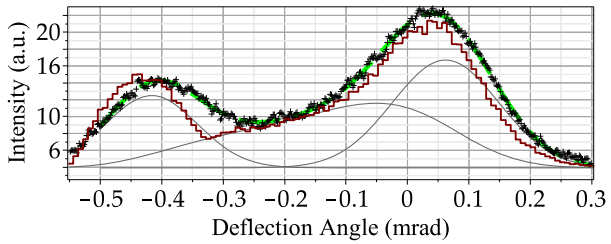

FIG. 4 (color online). Example of the fit to 3.35 GeV channeling data at 0 mrad crystal angle. Plot symbols and lines have the same meaning as in Fig. 3. For this example, the channeling efficiency is 22%, the surface transmission is 62%, and the dechanneling length is 38 μm.

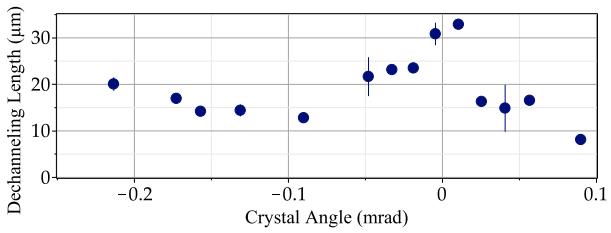

FIG. 5 (color online). Dechanneling length versus crystal angle, 6.3 GeV. Error bars reflect the scattering of the underlying data from several frames; the data points at −0.05 and +0.045 mrad have larger uncertainty due to beam jitter.

since particles identified as being in the dechanneling tail are not counted (see Figs. 3 and 4). Better indicating the operationally useable VR efficiency may be a fit to the reflected peak with an asymmetric Gaussian, which includes a certain fraction of the partially reflected particles. This gives the higher numbers shown in Table I. The apparent reduction at lower energy arises from the increased multiple scattering, which leads to the VR peak merging with the rechanneled peak in the VR orientation.

The results of the experiment are summarized in Table I. Errors are statistical but include variations between multiple frames, where applicable. The simulation results, as well as the histogram in Figs. 3 and 4, were obtained using the code DYNECHARM++ [31,32]. This code solves the equation of motion in the noninertial reference frame orthogonal to the crystal plane via numerical integration under the continuum potential approximation. It takes into account incoherent scattering on nuclei and electrons, which causes particle dechanneling and rechanneling. A detailed comparison will be published in a separate paper; the agreement between simulation and experiment appears to be good although there are differences in the details.

Figure 6 shows our results for the dechanneling length together with data from previous experiments at lower beam energies. The figure combines data from experiments with straight crystals with our data from a bent crystal.

For positively charged particles, the correction for the bending radius of the dechanneling length is straightforward and would lead to a modification upwards of our numbers by 10% at 3.35 GeV and 20% at 6.3 GeV for comparison with those for straight crystals, too small to change any conclusion. This correction is based on a parabolic potential. For electrons, the same scaling should hold for the initial dechanneling process; however, as shown below, rechanneling is an important process even at our beam energies. No published model exists for the effect of the bending on the rechanneling probability. Simulation results such as shown in Table I of Ref. [8] suggest a stronger dependence but are for much lower energy. In addition, we have evidence that the multiple scattering increases in an energy-dependent way for channeled particles relative to the scattering in the amorphous condition, further modifying the scaling of the dechanneling length with energy (see below). Carrigan [34] has discussed the dechanneling length of negatively charged particles and concludes that, while it is much shorter than for positively charged particles mostly due to increased multiple scattering, the dechanneling length for negatively charged particles should still scale with energy. Even with the above caveat, however, we believe our data are not consistent with this assertion. For the stated reasons we refrain from comparing our data with the scaling formula by Baier, Katkov, and Strakhovenko [35].

There is a discrepancy between the extracted dechanneling length and surface transmission and the intensity in the channeling peak. At 6.3 GeV, for a dechanneling length of 33 μm there should be 16% particles left in the channel at the end of the crystal. Multiplied by the surface transmission of 57% it would follow that the channeling efficiency would be less than 10% whereas we measure 22%. This indicates that the exponential model (1) used to describe dechanneling is overly simple. Calculations by the Frankfurt group for electron channeling at 855 MeV in Si (110) [23] as well as Baryshevsky *et al.* [36] show that rechanneling is an important process and that a simple exponential decay is not a good description of the process. Rather, at least a second much larger dechanneling length seems to be needed to describe the results. Recent measurements at Mainz [8] corroborate this. While these

TABLE I. Channeling parameters measured.

Parameter	Unit	3.35 GeV	Simulation	6.3 GeV	Simulation
Chann. effi.	%	22 ± 1	21	22 ± 1	20
Surf. Trans.	%	64 ± 2	67	57 ± 2	53
Dech. length	μm	43 ± 6	42	$33 + 5 - 2$	31
VR deflect.	μrad	120 ± 2	⋯	80 ± 1	⋯
VR effi.	%	61 ± 2	⋯	63 ± 2	⋯
(Alt. meth.)[a]		86 ± 1		95 ± 1	

[a]Different method of VR efficiency analysis, see text.

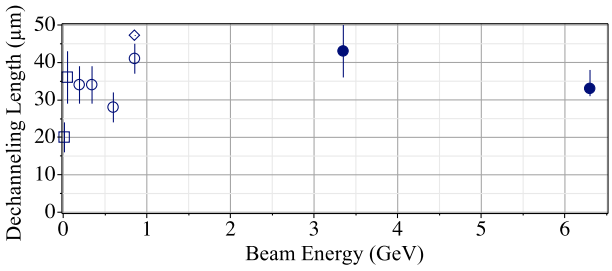

FIG. 6 (color online). Published data for the dechanneling length of electrons in Si crystals. The two open boxes indicate data for (110) planar channeling in straight crystals [33]; the open circles, (110) straight crystal [7]; the open diamonds, (111) straight crystal ([8] Table 1); the solid circles are this work, (111) bent crystal.

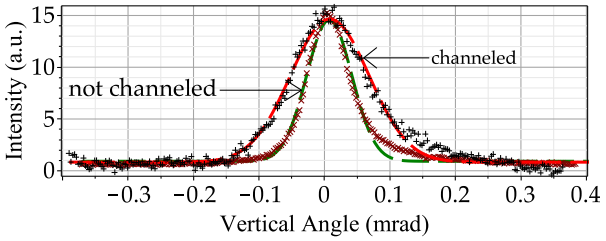

FIG. 7 (color online). Vertical profiles of channeled (black +) and not-channeled (brown ×) beam at 6.3 GeV together with Gaussian fits (dashed lines). The 1σ width of the channeled particles is 60 μrad, while the 1σ width of the not-channeled particles is 35 μrad, consistent with 39 μrad from the multiple-scattering formula [38]. The data sets are intensity normalized to each other.

particular calculations were done for a different energy and channeling plane, our data point in a similar direction.

There is a detectable increase in the width of the channeled beam in the vertical, nonchanneling plane over the width in the amorphous—or in the VR—orientation of the crystal. Figure 7 shows the vertical profile of the channeling peak at 6.3 GeV together with the vertical distribution for not-channeled particles. Expressing this increase in terms of the radiation length X_0 we get a reduction by a factor of 1.9 at 3.35 GeV, and 2.4 at 6.3 GeV. This effect can be explained qualitatively by the increased probability of the channeled electrons to overlap with the nuclei of the crystal lattice; to our knowledge the result reported here is the first published, quantitative result of this kind. A recent measurement at 255 MeV using a straight crystal does not appear to show this effect [37]. The DYNECHARM++ simulations mentioned above show a similar effect.

For the first time, channeling and volume reflection has been demonstrated with a full primary beam of multi-GeV electrons. The experimental data show that channeling happens with 22% efficiency and a surface transmission of 57%–64% for our crystal. The dechanneling length is 33–43 μm, and up to 6.3 GeV our data indicate little or no energy dependence of the dechanneling length. There is evidence for dechanneling not being a purely exponential process and that rechanneling is an important process in determining the overall channeling efficiency even at our energies, and that the dechanneling length is shorter for volume-captured particles. Volume reflection appears to be an efficient process with effectively more than 90% of electrons found in the volume-reflected ensemble. There is evidence of increased multiple scattering when channeling, in accordance with expectation but quantitatively reported here for the first time.

The results presented here provide a first quantitative look at the processes important in channeling and VR of a high-energy electron beam and thus crucial data to the further understanding and application of crystals for electron beams. The results provide important benchmark data for simulation codes; preliminary comparison to one such code indicates broad overall agreement with more detailed comparisons to follow. The results also provide data on which a first, cautious, extrapolation can be attempted to investigate the possibility of using crystal arrays in the VR orientation as collimators in electron-beam machines.

We would like to thank the SLAC Test Facilities Department for outstanding support in getting the experiment installed, and for data acquisition support and setting up the beam line. We would like to thank G. Frequest of Fogale Nanotech (Nimes, France) for his support in measuring the crystal thickness and P. Andrea and M. Claudio of Perman (Loiano, Italy) for their support with crystal cell manufacturing. We would like to thank E. L. Bong (SLAC) for designing and building the mount for the stages and crystal assembly. This work was partially supported by the U.S. DOE under Contract No. DE-AC02-76SF00515, by the U.S. National Science Foundation (Grant No. PHY-1068662), by the Danish Council for Independent Research—Natural Sciences FNU, and the Italian Istituto Nazionale di Fisica Nucleare (INFN) through the CHANEL experiment.

*uli@slac.stanford.edu

[1] See U. Uggerhøj, Rev. Mod. Phys. **77**, 1131 (2005) and references therein.
[2] See A. G. Afonin *et al.*, Phys. Rev. ST Accel. Beams **15**, 081001 (2012) and references therein.
[3] W. Scandale *et al.*, Phys. Rev. ST Accel. Beams **11**, 063501 (2008).
[4] R. Carrigan *et al.*, Phys. Rev. ST Accel. Beams **5**, 043501 (2002).
[5] D. Still *et al.*, *Proc. IPAC 2012, New Orleans, Louisiana, USA*, 559 (2012), http://accelconf.web.cern.ch/AccelConf/IPAC2012/papers/moppd082.pdf.
[6] R. P. Fliller III, A. Drees, D. Gassner, L. Hammons, G. McIntyre, D. Trbojevic, V. Biryukov, Y. Chesnokov, and V. Terekhov, *Proc. Part. Accel. Conf. Chicago, IL*, (IEEE, New York, 2001), p. 1399.
[7] W. Lauth, H. Backe, P. Kunz, and A. Rueda, Int. J. Mod. Phys. A **25**, 136 (2010).
[8] A. Mazzolari *et al.*, Phys. Rev. Lett. **112**, 135503 (2014).
[9] W. Scandale *et al.*, Phys. Lett. B **693**, 545 (2010).
[10] W. Scandale *et al.*, Phys. Lett. B **681**, 233 (2009).
[11] W. Scandale *et al.*, Phys. Rev. A **79**, 012903 (2009).
[12] L. Bandiera *et al.*, Nucl. Instrum. Methods Phys. Res., Sect. B **309**, 135 (2013).
[13] L. Bandiera, E. Bagli, V. Guidi, A. Mazzolari, A. Berra, D. Lietti, M. Prest, E. Vallazza, D. De Salvador, and V. Tikhomirov, Phys. Rev. Lett. **111**, 255502 (2013).
[14] V. B. S. Strokov, V. Biryukov, Yu. Chesnokov, I. Endo, M. Iinuma, H. Kuroiwa, T. Ohnishi, H. Sato, S. Sawada, T. Takahashi, and K. Ueda, J. Phys. Soc. Jpn. **76**, 064007 (2007).

[15] A. Seryi, Nucl. Instrum. Methods Phys. Res., Sect. A **623**, 23 (2010).
[16] M. Koratzinos *et al.*, *Proc. Int. Part. Accel. Conf. Shanghai, CN* (2013), p. 1658, http://accelconf.web.cern.ch/AccelConf/IPAC2013/papers/tupme040.pdf.
[17] S. Geer, Annu. Rev. Nucl. Part. Sci. **59**, 347 (2009).
[18] M. A. Palmer *et al.*, *Proc. Int. Part. Accel. Conf., Shanghai, CN* (2013), p. 1475, http://accelconf.web.cern.ch/AccelConf/IPAC2013/papers/tupfi057.pdf.
[19] J. Welch (private communication).
[20] B. Azadegan, W. Wagner, and J. Pawelke, Phys. Rev. B **74**, 045209 (2006).
[21] W. Wagner, B. Azadegan, A. Panteleeva, J. Pawelke, and W. Enghardt, Proc. SPIE Int. Soc. Opt. Eng. **5974**, 59740B (2005).
[22] T. N. Wistisen, K. K. Andersen, S. Yilmaz, R. Mikkelsen, J. Lundsgaard Hansen, U. I. Uggerhøj, W. Lauth, and H. Backe, Phys. Rev. Lett. **112**, 254801 (2014).
[23] G. B. Sushko, V. G. Bezchastnov, I. A. Solov'yov, A. V. Korol, W. Greiner, and A. V. Solov'yov, J. Comput. Phys. **252**, 404 (2013).
[24] V. Guidi, A. Mazzolari, D. De Salvador, and A. Carnera, J. Phys. D **42**, 182005 (2009).
[25] P. A. Doyle and P. S. Turner, Acta Crystallogr. A **24**, 390 (1968).
[26] http://estb.slac.stanford.edu.
[27] A. Murokh, J. Rosenzweig, V. Yakimenko, E. Johnson, and X. J. Wang, in *Proc. 2nd ICFA Advanced Accelerator Workshop, UCLA, Los Angeles, 1999* (World Scientific, Hong Kong, 2000) p. 564.
[28] A. H. Lumpkin, B. X. Wang, W. J. Berg, M. White, J. W. Lewellen, and S. V. Milton, Nucl. Instrum. Methods Phys. Res., Sect. A **429**, 336 (1999).
[29] A. Baurichter *et al.*, Nucl. Instrum. Methods Phys. Res., Sect. B **164–165**, 27 (2000).
[30] A. M. Taratin and S. A. Vorobiev, Nucl. Instrum. Methods Phys. Res., Sect. B **26**, 512 (1987).
[31] E. Bagli, V. Guidi, and V. A. Maisheev, Phys. Rev. E **81**, 026708 (2010).
[32] E. Bagli and V. Guidi, Nucl. Instrum. Methods Phys. Res., Sect. B **309**, 124 (2013).
[33] J. O. Kephart, R. H. Pantell, B. L. Berman, S. Datz, H. Park, and R. K. Klein, Phys. Rev. B **40**, 4249 (1989).
[34] R. A. Carrigan, Int. J. Mod. Phys. A **25**, 55 (2010).
[35] V. N. Baier, V. M. Katkov, and V. M. Strakhovenko, *Electromagnetic Processes at High Energies in Oriented Single Crystals* (World Scientific, Singapore, 1998).
[36] V. G. Baryshevsky and V. V. Tikhomirov, Nucl. Instrum. Methods Phys. Res., Sect. B **309**, 30 (2013).
[37] Y. Takabayashi, Yu. L. Pivovarov, and T. A. Tukhfatullin, Phys. Lett. A **378**, 1520 (2014).
[38] J. Beringer *et al.* (Particle Data Group), Phys. Rev. D **86**, 010001 (2012).